

# Spectral Distribution of Exceptional Points in Lattices with Localized Loss

J. R. SILVA

*Instituto de Física, Universidade Federal de Alagoas, Maceió, 57072-900, Brazil.*

*Corresponding author: jefferson.rocha@fis.ufal.br*

*Compiled January 15, 2026*

We explore the existence and stability of exceptional points (EPs) in finite waveguide arrays subject to single-site dissipation. We show that the EP landscape is dictated by a geometry-dependent parity effect, leading to strictly distinct spectral behaviors for arrays with even versus odd numbers of waveguides. Through analytical derivation and numerical analysis, we define the conditions under which these singularities emerge and evolve. Our findings clarify the mechanisms of symmetry breaking in finite non-Hermitian lattices, offering new guidelines for the design of robust optical structures that exploit or avoid exceptional points.

<http://dx.doi.org/10.1364/ao.XX.XXXXXX>

The study of non-Hermitian systems has evolved from a mathematical curiosity into a cornerstone of advanced optical engineering. Unlike conventional quantum mechanics, non-Hermitian optics explores open interactions via gain and loss, enabling novel phenomena such as unidirectional invisibility [1, 2] and single-mode lasers [3, 4]. Central to these advancements are Exceptional Points (EPs) [5–8], spectral singularities where eigenvalues and eigenvectors coalesce, resulting in an incomplete basis degeneracy.

The non-trivial topology surrounding EPs induces a drastic sensitivity to perturbations, which is fundamental for next-generation optical sensors. Coupled waveguide arrays have established themselves as an ideal platform to investigate this dynamics, allowing for precise control over coupling and the introduction of dissipation to simulate non-Hermitian Hamiltonians.

Current literature predominantly focuses on high-symmetry configurations, such as  $\mathcal{PT}$ -symmetric dimers or infinite lattices [9–11]. However, the spectral behavior of finite lattices with strictly localized dissipation remains largely unexplored. The symmetry breaking introduced by a dissipative impurity generates spectral complexities not captured by simplified models. Understanding how the spatial position of the loss affects the distribution of EPs is crucial for designing photonic circuits where localized dissipation is either inevitable or intentional for mode filtering [12, 13]. In this work, we systematically analyze the formation and distribution of EPs in finite arrays of  $N$  coupled waveguides perturbed by localized dissipation. By treating the

loss site position and system size as control parameters, we reveal that the emergence of EPs is not random but follows strict geometric patterns governed by the lattice's discrete symmetries including a notable parity effect depending on whether  $N$  is even or odd. We demonstrate, analytically and numerically, that the location of these singularities in parameter space is deterministic and predictable. Our results map the phase diagram of these discrete lattices, offering new guidelines for the robust control of light states in structured dissipative systems.

Initially, we built a list of single-mode coupled waveguides,  $G_1, G_2, \dots, G_{N-1}, G_N$ , where, for some  $j$ ,  $G_j$  has a loss to the environment that can be mapped by a reservoir Markovian.

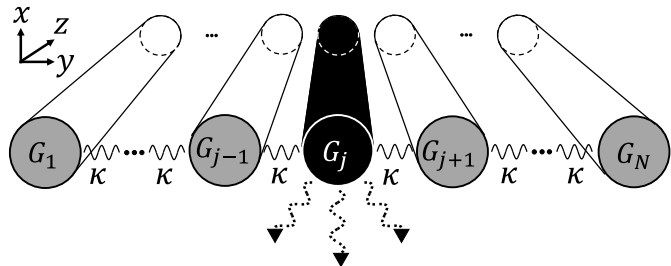


**Fig. 1.** Sequence with  $N$  coupling waveguides, with coupling constant  $\kappa$ , where the waveguide  $G_j$  has Markovian loss indicated by the dashed arrows.

The Hamiltonian of the set of coupled guides observed in figure 1, in the RWA approximation, is described for  $H_G$  with the presence of the environment

$$H_G = \beta \sum_{m=1}^N a_m^\dagger a_m + \kappa \sum_{0 < l < N} (a_l^\dagger a_{l+1} + a_l a_{l+1}^\dagger), \quad (1)$$

where  $\beta$  and  $\kappa$  denote the propagation constants and the mutual coupling between the waveguides, respectively, and  $a_m$  and  $a_m^\dagger$  represent the annihilation and creation operators for waveguide  $m$  in the standard Schrödinger picture. The effective Hamiltonian, derived by integrating out the reservoir degrees of freedom, i.e., assuming the Markovian limit and performing the trace over the environment, is given by

$$H_{\text{eff}} = H_G - i\sigma a_j^\dagger a_j, \quad (2)$$

with  $\sigma$  being a constant associated with the loss rate.

In the Heisenberg picture, we write the spatial evolution equations for the annihilation operators of each waveguide in the system using the coupled equation

$$\frac{d}{dz} \begin{bmatrix} a_1 \\ \vdots \\ a_N \end{bmatrix} = -i \begin{bmatrix} \beta_1 & \kappa & & \\ \kappa & \ddots & \ddots & \\ & \ddots & \ddots & \kappa \\ & & \kappa & \beta_N \end{bmatrix} \begin{bmatrix} a_1 \\ \vdots \\ a_N \end{bmatrix} \quad (3)$$

where  $\beta_m = \beta - i\delta_{jm}\sigma$ , indicating the presence of Markovian loss in waveguide  $G_j$ . To solve the system given by  $da/dz = -iMa$ , we move to the Laplace domain, variable  $s$ , and transform back to the spatial domain  $z$  via  $a(z) = \mathcal{L}^{-1}\{(s + iM)^{-1}\}a(0)$ ; thus, each entry of  $a(z)$  takes the form

$$a_m(z) = e^{-i\beta z} \sum_{k=1}^N f_{mk}^{(j)}(z) a_k(0). \quad (4)$$

The squared modulus of the amplitude  $f_{mk}^{(j)}(z)$  physically represents the relative fraction of the average photon number in waveguide  $G_m$  at position  $z$  when photons are launched into waveguide  $G_k$  at  $z = 0$ , with loss present in waveguide  $G_j$ . In the lossless case ( $\sigma = 0$ ),  $f^{(j)} \equiv f$  takes the well-known form

$$f_{mk}(z) = \frac{2}{N+1} \sum_{n=1}^N \sin\left(\frac{kn\pi}{N+1}\right) \sin\left(\frac{mn\pi}{N+1}\right) e^{-i\lambda_n z} \quad (5)$$

where  $\lambda_n = 2\kappa \cos[n\pi/(N+1)]$  are the eigenvalues of the Hermitian Hamiltonian; thus, the periodic nature of these functions is observed only for  $N = 2$  and  $N = 3$ , since the projection of the angular spectrum is equispaced.

In the presence of loss in waveguide  $G_j$ , we present the coefficients of Eq. Eq. (4) in the Laplace domain with  $m \geq k$

$$f_{mk}^{(j)}(z) = i^{k-m} \mathcal{L}^{-1} \begin{cases} \theta_{N-m} \frac{\theta_{k-1} + (\sigma/\kappa) \theta_{j-1} \theta_{k-j-1}}{\theta_N + (\sigma/\kappa) \theta_{j-1} \theta_{N-j}}, & m > j \\ \theta_{N-m} + (\sigma/\kappa) \theta_{j-m-1} \theta_{N-j}, & m \leq j \end{cases} \quad (6)$$

where  $\theta_m = \theta_m(s/\kappa)$  denotes the Fibonacci polynomials, defined by  $\theta_0(x) = 1$ ,  $\theta_1(x) = x$ , and the recurrence relation  $\theta_m(x) = x\theta_{m-1}(x) + \theta_{m-2}(x)$  for higher orders

$$\begin{aligned} \theta_2(x) &= x^2 + 1 \\ \theta_3(x) &= x^3 + 2x \\ \theta_4(x) &= x^4 + 3x^2 + 1 \\ &\vdots \\ \theta_N(x) &= \sum_{m=0}^{\lfloor N/2 \rfloor} \binom{N-m}{m} x^{N-2m} \end{aligned} \quad (7)$$

We observe that Eq. Eq. (6), at  $\sigma = 0$ , has the denominator  $\theta_N$  whose roots are  $\lambda_n$ , thus recovering the Hermitian case.

From the perspective of the tridiagonal matrix in Eq. (3), the proposed  $N$ -waveguide system has eigenvalues with associated

eigenspaces of dimension 1; this means that eigenvalue degeneracy directly implies eigenvector coalescence.

Equation Eq. (6) can be analytically written in position space using the partial fraction decomposition method, provided the roots of the polynomial  $\theta_N + (\sigma/\kappa) \theta_{j-1} \theta_{N-j}$  are known. EPs arise when this polynomial exhibits repeated roots. In this instance, we evaluate the system formed by the zeros of the described polynomial and its derivative, or equivalently, the points where  $\theta_N$  and  $\theta_{j-1} \theta_{N-j}$  are linearly dependent. The Wronskian follows from this discussion:

$$W_{N,j} = (\theta_{j-1} \theta_{N-j}) \theta'_N - (\theta_{j-1} \theta_{N-j})' \theta_N \quad (8)$$

The Wronskian possesses no free parameters other than  $N$  and  $j$ , allowing for the rapid detection of the critical rates  $\sigma$  at which exceptional points occur. The parity operation yields a physically equivalent system, an observation that follows from the index symmetry  $f_{N+1-k, N+1-m}^{(N+1-j)} = f_{m,k}^{(j)}$ . By virtue of this symmetry, we may restrict our analysis to cases where  $j \leq \lceil N/2 \rceil$ . Figure 2 displays the critical values of  $\sigma$  for given  $N$  and  $j$ .

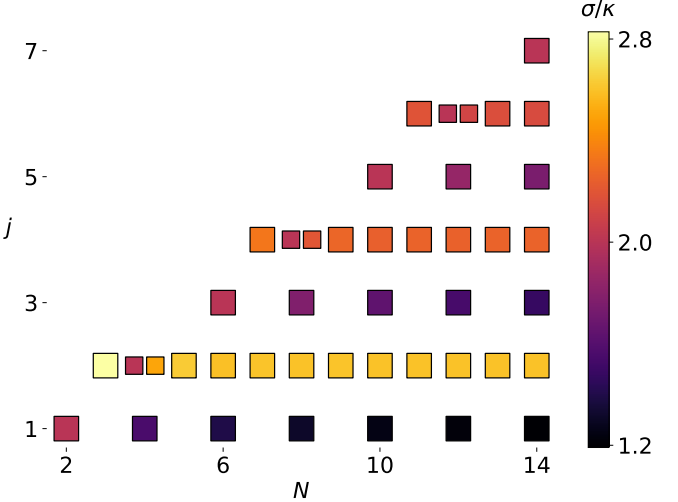


**Fig. 2.** Critical loss parameter  $\sigma/\kappa$  for a sequence of  $N$  guides with loss in guide  $G_j$ , with  $j \leq \lceil N/2 \rceil$ .

Note that simultaneously odd values of  $j$  and  $N$  do not admit a critical  $\sigma$ . Furthermore, an interesting phenomenon occurs for even  $N$  when loss is present in one of the central waveguides: the critical loss parameter satisfies  $\sigma = 2\kappa$ , a result inherited from the dimer case [14, 15]. Additionally, when  $j$  is even, we obtain an extra exceptional point (EP).

In the case of absent exceptional points in waveguides with  $j = 1$ , this can be justified by the existence of a zero mode that keeps its real part anchored at the center; while the lateral modes move, the central mode acts as a topological barrier. The lack of a partner for the central mode prevents typical coalescence. Still with  $j = 1$ , but for even  $N$ , the central eigenvalues merge to generate a zero mode—specifically, a mode confined to the imaginary axis—maintaining separation between the remaining modes.

For  $j \neq 1$ , we can view the system as a combination of two sublattices,  $[1, j]$  and  $[j, N]$ , with losses at the extremities. In this case, if the size of one of the sublattices ( $j$  or  $N - j$ ) is even, then exceptional points exist.

Observe that a system composed of an even number of waveguides with  $\sigma = 2\kappa$  and  $j = N/2$  renders the system

matrix non-diagonalizable; this choice fuses eigenvalues and eigenvectors in pairs. Note the common denominator of the amplitudes in the Laplace domain in Eq. Eq. (6):  $\sigma/\kappa = 2$  makes them perfect squares pointwise due to the relation:  $\theta_N + 2\theta_{N/2}\theta_{N/2-1} = (\theta_{N/2} + \theta_{N/2-1})^2$ .

For  $\sigma$  slightly larger, the eigenvalues separate again, except when one of the collapses occurs generating a zero mode. When  $N$  is even but not a multiple of 4, for example, the generation of the zero mode occurs immediately after  $\sigma = 2\kappa$ . Observe in Figure 3 the eigenvalues  $\lambda \approx \pm 1.30714 - 0.21508i$  and the formation of the zero mode at  $\lambda \approx -0.56984i$ .

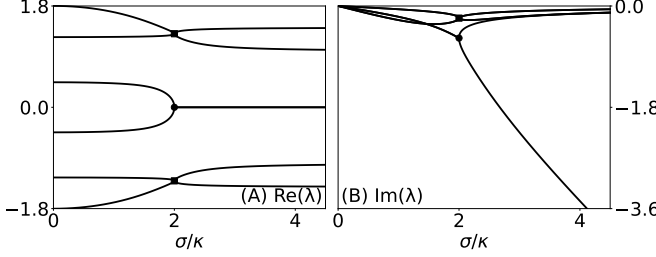


**Fig. 3.** Eigenvalue trajectories versus the loss ratio  $\sigma/\kappa$  for a chain with  $N = 6$  and loss at site  $j = 3$ . Panels (A) and (B) display the real and imaginary parts of the spectrum, respectively.

When  $N$  is a multiple of 4, a new EP emerges at  $\sigma > 2\kappa$ , yielding a zero mode, as shown in Fig. 4. We observe this phenomenon in panel (A) for the canonical case  $N = 4$ , where the eigenvalues are  $\lambda = i \exp(\pm 2\pi i/3)$  at  $\sigma = 2\kappa$ , while at  $\sigma = 2.5\kappa$ , they become  $i$  and  $[\pm\sqrt{15} + i]/4$ .

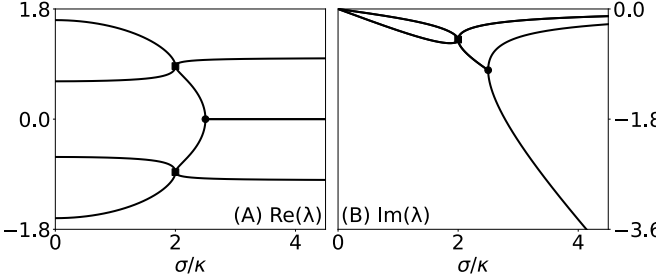


**Fig. 4.** Eigenvalue trajectories versus the loss ratio  $\sigma/\kappa$  for a chain with  $N = 4$  and loss at site  $j = 2$ . Panels (A) and (B) display the real and imaginary parts of the spectrum, respectively.

Localized loss serves as a mechanism for topological selection. At the boundary, it effectively reduces the system dimensionality ( $N \rightarrow N - 1$ ), compelling a global spectral redistribution that can reveal a topological zero mode. Conversely, bulk loss functions as an infinite potential barrier, splitting the chain into two independent subsystems where the existence of EPs or zero modes is dictated solely by the local geometry of the isolated sub-lattices.

To elucidate the EP dynamics, the system is extended by coupling an extra waveguide to guide  $G_N$ , yielding  $N + 1$  elements. This auxiliary guide possesses a coupling constant  $\alpha \neq \kappa$  and a loss rate  $\sigma = \gamma/2$ . In Laplace space, the determinant reads  $|s + iM| = (s + \gamma/2)\theta_N + \alpha^2\theta_{N-1}$ . The exceptional points of this extended system are parameterized by the double roots of

$(x - \gamma/2\kappa)\theta_N + \frac{\alpha^2}{\kappa^2}\theta_{N-1}$ , under the variable change  $x = -s/\kappa$ . The loss rate and the coupling strength are thus described by

$$\begin{cases} \frac{\gamma}{\kappa} = 2x + \frac{2\theta_N(x)\theta_{N-1}(x)}{\theta'_N(x)\theta_{N-1}(x) - \theta_N(x)\theta'_{N-1}(x)} \\ \frac{\alpha}{\kappa} = \frac{\theta_N(x)}{\sqrt{\theta'_N(x)\theta_{N-1}(x) - \theta_N(x)\theta'_{N-1}(x)}} \end{cases}, \quad (9)$$

Defining  $W = \theta'_N\theta_{N-1} - \theta_N\theta'_{N-1}$ , the parametrizations satisfy  $x > 0$  for odd  $N$  and  $x > W^{-1}(0)$  for even  $N$ .

The curve described by Eq. Eq. (9) traces the locus of repeated eigenvalues; Fig. 5 displays this boundary, which separates the eigenvalue classes [16, 17].

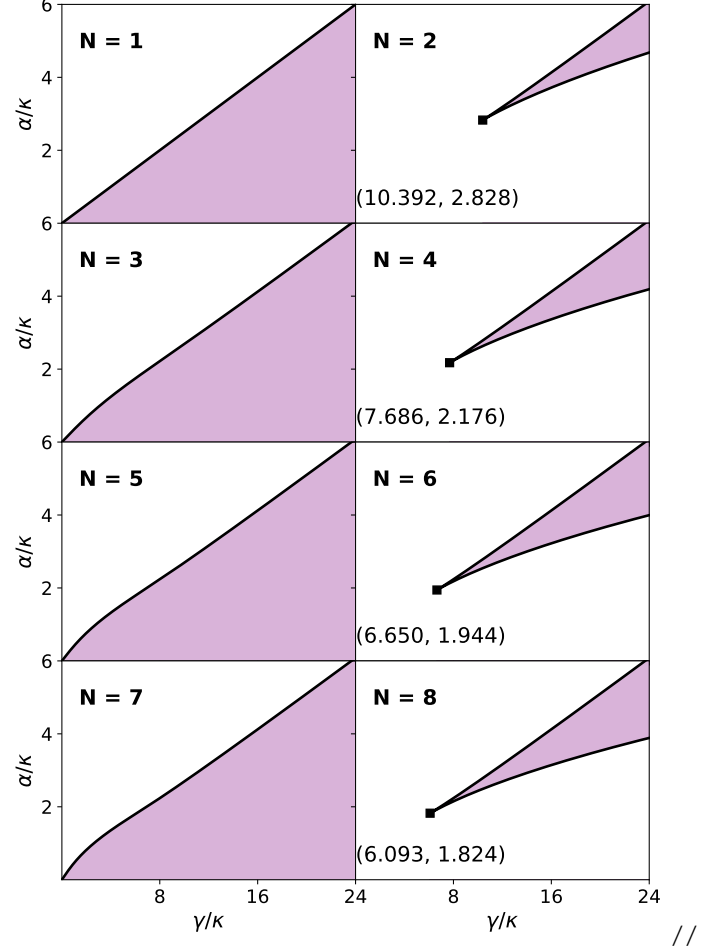


**Fig. 5.** Regions delineating the eigenvalue spectrum's nature. The purple shaded region denotes the environment with some purely imaginary eigenvalues.

For  $N = 1$ , eigenvector coalescence occurs along the line  $\alpha = \gamma/4$ . All odd- $N$  cases exhibit a partition of solution regions that appear as deformations of this initial case. In the horizontal line  $\alpha = \kappa$ , the intersection with the coalescence curve occurs at increasingly smaller  $\gamma$  values as  $N$  increases. This decrease is observed in panel  $j = 1$  of Fig. 2.

The even- $N$  cases are more peculiar, featuring a coalescence point of three eigenvalues (EP3). This triple root occurs when the parameterization in Eq. Eq. (9) reaches a critical point, satisfying  $\frac{d\alpha}{dx} = 0 = \frac{d\gamma}{dx}$ . With some algebra, this corresponds to  $x =$

$\left[ \frac{d^2}{dx^2} \frac{\theta_{N-1}}{\theta_N} \right]^{-1}(0)$ . We can tabulate these values and observe an apparent decrease for this special point."

**Table 1.** Simultaneous coalescence points of three eigenvalues.

$N$	$x$	$\gamma/\kappa$	$\alpha/\kappa$
2	1.7320508076	10.392304845413	2.82842712475
4	1.1631827081	7.685672761047	2.17568084056
6	0.9027678865	6.649939740468	1.9439583753
8	0.7477721104	6.092654106580	1.82414907376
10	0.6431138119	5.740902957312	1.75050496066
12	0.5669207624	5.497106462282	1.70044050968
14	0.5085871334	5.317379517210	1.66407883274
16	0.4622814204	5.178951502979	1.63640404897
18	0.4245053279	5.068784002605	1.61459330451

In the limit of arbitrarily large  $N$ , the coordinate  $x$  corresponding to the triple eigenvalue merger tends to zero. Through an asymptotic expansion of the Fibonacci polynomials in Eq. (9), we yield the limiting values  $\gamma \rightarrow 4\kappa$  and  $\alpha \rightarrow \sqrt{2}\kappa$ . These asymptotic results underpin the physical interpretation of the system beyond a simple linear chain.

By restricting our analysis to the  $N$  functional elements, we observe that the additional dissipative waveguide effectively acts as a tunable Lorentzian reservoir, where  $\gamma$  represents the full width at half maximum (FWHM) of the distribution [17, 18]. Unlike a passive drain that merely absorbs energy, this reservoir modifies the main chain's spectral topology, enabling the manipulation of Exceptional Points and the transition between absorption and reflection regimes.

This reservoir perspective elucidates the mechanism behind the dissipative Zeno effect [19, 20]: the mismatch imposed by the Lorentzian reservoir creates an effective barrier, confining the dynamics within the original  $N$  waveguides. Therefore, our study confirms that the controlled introduction of non-Hermiticity via artificial reservoirs offers a robust degree of freedom for spectral engineering, allowing finite waveguide chains to exhibit complex behaviors typically associated with much larger or continuous systems.

## ACKNOWLEDGMENTS

The author acknowledge the financial support of CNPq (Conselho Nacional de Desenvolvimento Científico e Tecnológico), CAPES (Coordenação de Aperfeiçoamento de Pessoal de Nível Superior) and FAPEAL (Fundação de Amparo à Pesquisa do Estado de Alagoas).

## DISCLOSURES

The author declare no conflicts of interest.

## REFERENCES

1. Z. Lin, H. Ramezani, T. Eichelkraut, *et al.*, *Phys. Rev. Lett.* **106**, 213901 (2011).
2. L. Feng, Y.-L. Xu, W. S. Fegadolli, *et al.*, *Nat. materials* **12**, 108 (2013).
3. L. Feng, Z. J. Wong, R.-M. Ma, *et al.*, *Science* **346**, 972 (2014).
4. H. Hodaei, M.-A. Miri, M. Heinrich, *et al.*, *Science* **346**, 975 (2014).
5. M.-A. Miri and A. Alu, *Science* **363**, eaar7709 (2019).
6. W. D. Heiss, *J. Phys. A: Math. Theor.* **45**, 444016 (2012).
7. F. U. Klauck, M. Heinrich, A. Szameit, and T. A. Wolterink, *Sci. Adv.* **11**, eadr8275 (2025).
8. E. J. Bergholtz, J. C. Budich, and F. K. Kunst, *Rev. Mod. Phys.* **93**, 015005 (2021).
9. C. E. Rüter, K. G. Makris, R. El-Ganainy, *et al.*, *Nat. physics* **6**, 192 (2010).
10. L. Ge, *Phys. Rev. A* **92**, 052103 (2015).
11. L. Xue, Z. Gong, H. Zhu, and Z. Wang, *Opt. Express* **25**, 17249 (2017).
12. L. Feng, R. El-Ganainy, and L. Ge, *Nat. Photonics* **11**, 752 (2017).
13. J. Wiersig, *Photonics research* **8**, 1457 (2020).
14. P. C. Burke, J. Wiersig, and M. Haque, *Phys. Rev. A* **102**, 012212 (2020).
15. S. Longhi, *Opt. Lett.* **43**, 5371 (2018).
16. F. Cavaliere, G. Gemme, G. Benenti, *et al.*, *Commun. Phys.* **8**, 76 (2025).
17. J. Silva and P. Brandão, *J. Opt.* **27**, 105201 (2025).
18. G. Mouloudakis, T. Ilias, and P. Lambropoulos, *Phys. Rev. A* **105**, 012429 (2022).
19. K. Snizhko, P. Kumar, and A. Romito, *Phys. review research* **2**, 033512 (2020).
20. P. Facchi and S. Pascazio, *J. Phys. A: Math. Theor.* **41**, 493001 (2008).